© 2014. Published by The Company of Biologists Ltd | The Journal of Experimental Biology (2014) 217, 3085-3094 doi:10.1242/jeb.105676

RESEARCH ARTICLE

Hydrodynamics and energetics of jumping copepod nauplii and copepodids

Navish Wadhwa[1,*], Anders Andersen[1] and Thomas Kiørboe[2]

ABSTRACT

Within its life cycle, a copepod goes through drastic changes in size, shape and swimming mode. In particular, there is a stark difference between the early (nauplius) and later (copepodid) stages. Copepods inhabit an intermediate Reynolds number regime (between ~1 and 100) where both viscosity and inertia are potentially important, and the Reynolds number changes by an order of magnitude during growth. Thus we expect the life stage related changes experienced by a copepod to result in hydrodynamic and energetic differences, ultimately affecting the fitness. To quantify these differences, we measured the swimming kinematics and fluid flow around jumping *Acartia tonsa* at different stages of its life cycle, using particle image velocimetry and particle tracking velocimetry. We found that the flow structures around nauplii and copepodids are topologically different, with one and two vortex rings, respectively. Our measurements suggest that copepodids cover a larger distance compared to their body size in each jump and are also hydrodynamically quieter, as the flow disturbance they create attenuates faster with distance. Also, copepodids are energetically more efficient than nauplii, presumably due to the change in hydrodynamic regime accompanied with a well-adapted body form and swimming stroke.

KEY WORDS: Copepodids, Nauplii, Reynolds number, Swimming, Velocimetry, Energy dissipation

INTRODUCTION

Copepods are millimetre-sized crustaceans that are ubiquitous in both marine and freshwater aquatic systems. By some estimates, they are the most abundant metazoans in the oceans and form a vital part of the oceanic food web (Verity and Smetacek, 1996; Turner, 2004). Planktonic copepods are the dominant predator group for autotrophic and heterotrophic unicellular eukaryotes and a primary food source for higher trophic levels, such as planktivorous fish (Turner, 2004). As the biggest zooplankton group, copepods also provide an important link in the biogeochemical cycles. Thus, a good understanding of copepod ecology is essential for any attempt towards a holistic understanding of the aquatic ecosystems.

To feed, avoid predators and to find mates, a copepod must inevitably move through the water. However, there are costs associated with swimming, both in terms of energetic expenditures and in terms of predation risk, because fluid disturbances created by swimming copepods may signal their presence to rheotactic predators (Visser, 2001). Understanding and quantifying the trade-offs associated with fundamental activities, such as feeding and mate searching, allows predictions of optimal behaviours (Kiørboe and Jiang, 2013). Copepods inhabit an interesting intermediate Reynolds number range in between the low Reynolds number flows, which are dominated by viscous friction, characteristic of swimming microorganisms (Lauga and Powers, 2009), and the high Reynolds number flows, which are dominated by inertia, characteristic of larger organisms, such as swimming fish (Vogel, 1994). Previous studies involving intermediate Reynolds numbers have reported many interesting hydrodynamic phenomena, such as ciliary-to-flapping transition in molluscs (Childress and Dudley, 2004), change from viscous to inertial propulsion in ascidian larvae (McHenry et al., 2003) and rowing-to-flapping transition in a nymphal mayfly (Sensenig et al., 2009). Research on the hydrodynamics of swimming in adult copepods has revealed several important aspects of copepod locomotion, such as high swimming efficiency (Jiang and Kiørboe, 2011b), the formation of vortex rings (Yen and Strickler, 1996) and the resulting hydrodynamic camouflage (Jiang and Kiørboe, 2011a).

A little studied aspect of copepod swimming is the changes in hydrodynamic characteristics that take place during its development from egg to adult, a process associated with remarkable changes in size, morphology and swimming gait (Nybakken and Bertness, 2005). Copepods go through a number of intermediate developmental stages, each terminating with a moult. The first six stages are termed nauplius and the later six consist of five copepodid stages and the final adult form (Larink and Westheide, 2006). In many copepod species, both nauplii and adults swim in jumps, in which a quick power stroke is followed by a slow recovery stroke. In both nauplii and copepodids, swimming jumps involve a metachronal movement of the appendages and a simultaneous recovery (Andersen Borg et al., 2012; van Duren and Videler, 2003). The naupliar power stroke consists of the antennae moving backwards, followed by the antennules, both in a breaststroke-like fashion (Fig. 1A–F). In copepodids, the jumps are initiated by a downward movement of the first antennae, followed by a metachronal movement of the ventrally positioned swimming legs, which are all retracted together during the recovery stroke (Fig. 1G–L).

In this paper, we try to quantify the mechanistic changes experienced by a copepod during its life cycle, as it grows up from a nauplius to an adult. These changes are bound to affect the hydrodynamics of swimming and must have an effect on the Darwinian fitness of the organism. We consider the cost-side of swimming, i.e. the fluid disturbances generated and the energy expenditure. Specifically, we focus on the following questions: (i) how do the changes related to size and propulsion mode between the nauplii and copepodids affect the flow induced by the propulsion, (ii) how do the changes in flow structure affect the predation risk via the temporal and spatial attenuation of the induced disturbance and

[1]Department of Physics and Centre for Ocean Life, Technical University of Denmark, DK-2800 Kgs. Lyngby, Denmark. [2]National Institute for Aquatic Resources and Centre for Ocean Life, Technical University of Denmark, DK-2920 Charlottenlund, Denmark.

*Author for correspondence (nawa@fysik.dtu.dk)

Received 21 March 2014; Accepted 16 June 2014

The Journal of Experimental Biology (2014) doi:10.1242/jeb.105676

List of symbols and abbreviations

b	scaling exponent for spacial decay of flow disturbance
C_d	drag coefficient
D	equivalent sphere diameter for an organism
F_d	drag force
L	body length
M	carbon mass of an organism
n	number of jumps
N	sample size
p	pressure
P	rate of viscous energy dissipation
PIV	particle image velocimetry
PTV	particle tracking velocimetry
r	distance from the organism
R	size of the disturbance
R_0	size of the disturbance at the end of the power stroke
Re	Reynolds number
Re_s	instantaneous Reynolds number
R_m	mass specific metabolic rate
S	area of influence
S_0	area of influence at the end of the power stroke
T	duration of the power stroke
T_{decay}	decay time scale
T_{end}	total duration of motion
T_{visc}	viscous time scale
U	maximum swimming velocity
U_t	flow velocity threshold
$\mathbf{v}$	flow velocity
v_f	flow velocity magnitude
V	instantaneous swimming velocity
W_{diss}	energy dissipation per jump
W_{drag}	useful work per jump
β	frequency parameter
ε_{ij}	rate of strain tensor
μ	dynamic viscosity
ν	kinematic viscosity
ρ	fluid density
ϕ	viscous dissipation function

(iii) how does it affect the cost of propulsion? To answer these questions, we make measurements of the velocity fields around the naupliar and copepodid stages of the copepod *Acartia tonsa* (Dana 1849), using particle tracking velocimetry (PTV) and particle image velocimetry (PIV). We show that the flow structures around nauplii and copepodids are fundamentally different and that copepodids are hydrodynamically quieter than nauplii. We also measure the viscous energy dissipation around the jumping copepods, and we show that the energetic efficiency of swimming is smaller for nauplii than for copepodids.

RESULTS

Flows created by jumping nauplii and copepodids

For a straight jump of a nauplius, the flow was approximately left–right symmetric with respect to the body axis at all times (Fig. 2). The insets in Fig. 2 correspond to the different stages of the jump shown in Fig. 1. Given the measurement noise, the dominant flow structure is hard to see at the beginning of the stroke (Fig. 2A,B), but in the later part of the power stroke, a strong circulation was seen on each side of the organism (Fig. 2C). The spatial extent of the structure was at its maximum at the end of the power stroke, when the antennules finished their beat (Fig. 2D). During the recovery stroke (Fig. 2E,F), the flow structure started dissipating and it had diminished considerably by the end of the recovery stroke, when the antennae and the antennules returned to their original positions. We observed qualitatively the same flow structure in all our observations, also when nauplii were swimming with the lateral side facing the camera. Thus, the observed flow structure, with its two regions of opposite circulation, is in fact a cross-section of a toroidal vortex ring. The axis of the ring was aligned with the swimming direction.

For copepodids, the observed flow structure was qualitatively different from that around nauplii. Instead of two, four regions of circulation were seen, two in the front and two in the wake of the organisms (Fig. 3). The same qualitative structure was observed in the dorsal and the lateral view, although we only included lateral view in our study because when viewed dorsally, copepods tended to jump out of the measurement plane. The copepodid jump thus resulted in two counter-rotating vortex rings (Fig. 3), one in the front and another in the wake of the organism. A strong backwards jet was observed towards the end of the power stroke (Fig. 3D).

The distinction between the flow structure around a jumping nauplius and a copepodid was consistent through the various development stages, as highlighted in Fig. 4, which shows the flow fields around differently sized nauplii and copepods at the end of the power stroke. The flow-fields around nauplii and copepodids were topologically different. While the nauplii had a single vortical structure around the body when they jumped, the copepodids had two of them.

Reynolds number versus frequency parameter

The flows due to swimming nauplii and copepodids are described by the Navier–Stokes equation and the continuity equation for a Newtonian and incompressible fluid:

$$\rho\left(\frac{\partial \mathbf{v}}{\partial t}+(\mathbf{v}\cdot\nabla)\mathbf{v}\right)=-\nabla p+\mu\nabla^2\mathbf{v}\,, \qquad (1)$$

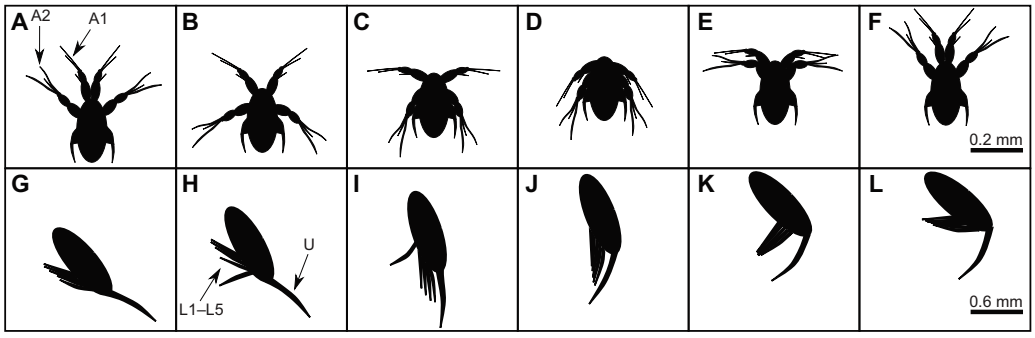

Fig. 1. Jumps of a nauplius and a copepodid. Series of snapshots showing the jump of a nauplius (A–F) and a copepodid (G–L). The first four panels in both rows show the power stroke, and the last two show the recovery stroke. The *Acartia tonsa* nauplius uses its antennules (A1) and antennae (A2) for propulsion (Andersen Borg et al., 2012). The copepodid uses its swimming legs (L1–L5) for propulsion and the urosome (U) for steering (Kiørboe et al., 2010). Copepodids have a variable number of pairs of swimming legs, and the final adult stage is shown here. The feeding appendages and the antennae are not shown for clarity.

The Journal of Experimental Biology (2014) doi:10.1242/jeb.105676

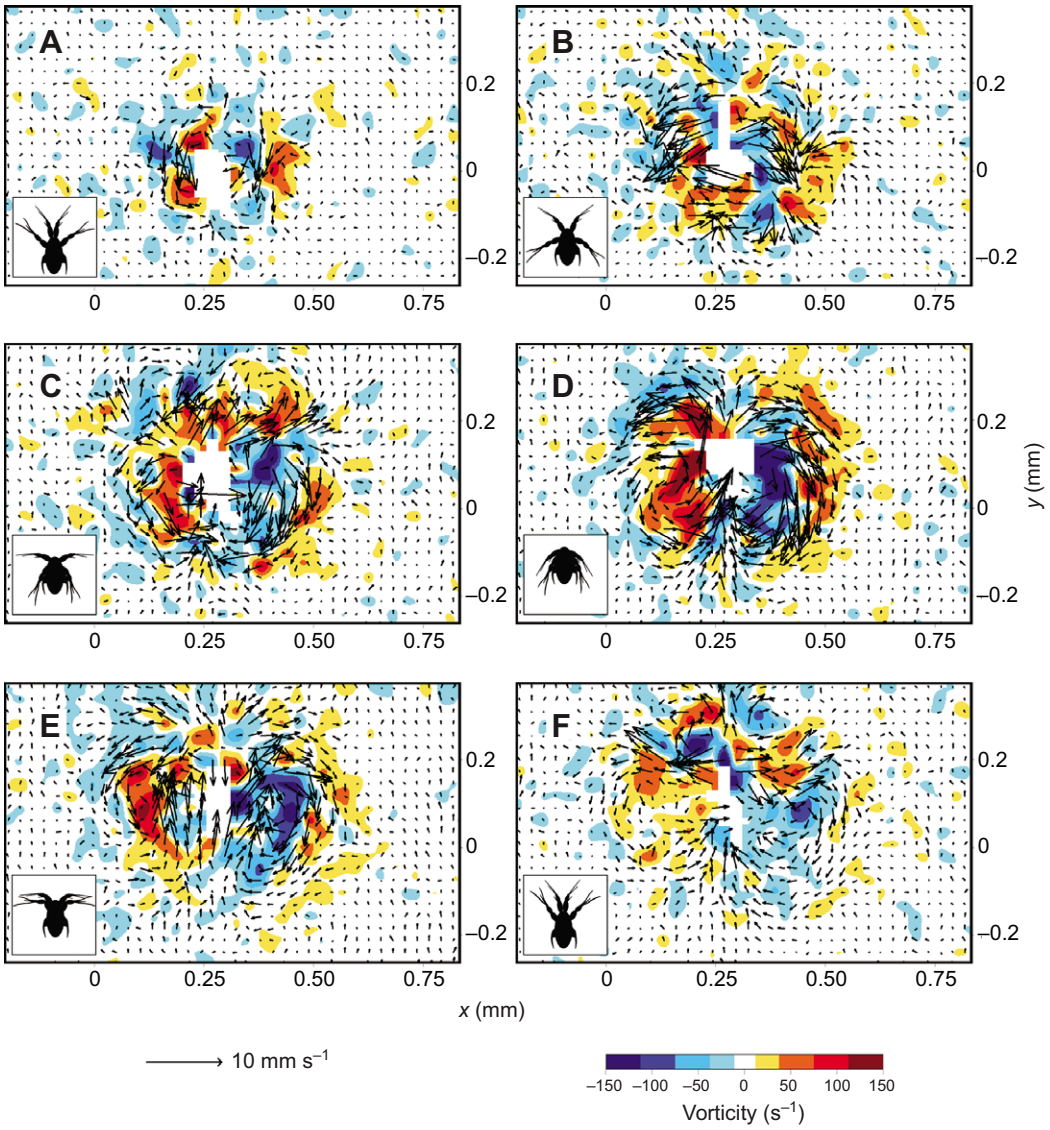

Fig. 2. Time series of the flow fields around a jumping nauplius. L=0.24 mm, T=7.5 ms, U=33.7 mm s^{-1}, β=7.4, Re=7.7. The position of the appendages is shown in the insets and correspond to the stages in Fig. 1. The arrows represent velocity vectors and the colours vorticity, with warm colours for counter-clockwise rotation and cool colours for clockwise rotation. (A–D) A toroidal vortex ring forms during the power stroke, and the maximum velocity is attained. (E,F) During the recovery stroke, the vortex ring is dissipated. Also see supplementary material Movie 1.

$$\nabla \cdot \mathbf{v} = 0\,, \tag{2}$$

where $\mathbf{v}$ is the velocity field, p is the pressure field, ρ is the fluid density and μ is the dynamic viscosity. The governing equations can be written in dimensionless form by introducing dimensionless variables:

$$\hat{\mathbf{x}}=\frac{\mathbf{x}}{L},\quad \hat{t}=\frac{t}{T},\quad \hat{\mathbf{v}}=\frac{\mathbf{v}}{U},\quad \hat{p}=\frac{L\,p}{\mu U}\,, \tag{3}$$

where L is the characteristic length scale, T the characteristic time scale and U the characteristic velocity scale. Using the dimensionless variables, we can write the governing equations:

$$\beta\frac{\partial\hat{\mathbf{v}}}{\partial\hat{t}}+Re(\hat{\mathbf{v}}\cdot\hat{\nabla})\hat{\mathbf{v}}=-\hat{\nabla}\hat{p}+\hat{\nabla}^2\hat{\mathbf{v}}\,, \tag{4}$$

$$\hat{\nabla}\cdot\hat{\mathbf{v}}=0\,, \tag{5}$$

where we have defined the two dimensionless parameters:

$$\beta=\frac{L^2}{\nu T}\,, \tag{6}$$

$$Re=\frac{LU}{\nu}\,. \tag{7}$$

Here, ν is the kinematic viscosity defined as ν=μ/ρ. The parameter β is often referred to as the frequency parameter (Pozrikidis, 2011) and Re is the Reynolds number. To describe the swimming nauplii and copepodids, we used body length as the characteristic length scale L, the duration of the power stroke as the characteristic time scale T and the maximum swimming velocity during a jump as the characteristic velocity scale U. It is natural to regard the frequency parameter β as characterizing the motion of the swimming appendages during the power stroke, and to think of the Reynolds number Re as describing the resulting swimming motion (Childress and Dudley, 2004).

The Re and β data for nauplii and copepodids (Fig. 5; Table 1) segregated into two distinguishable groups – nauplii at lower values of both β and Re, and copepodids at higher values of β and Re. At low Reynolds numbers, swimming velocity is proportional to the swimming appendage speed, resulting in a direct proportionality between β and Re (Lauga and Powers, 2009). In the case of nauplii, there was indeed a strong one-to-one relationship between β and Re (Fig. 5, inset). A straight line fit of nauplii data forced through the origin (solid line) had a slope of 1.09±0.06 (95% confidence interval). A linear fit between β and Re for copepodids (dashed line) had a slope of 1.75±0.59, higher than that for nauplii data.

The Journal of Experimental Biology (2014) doi:10.1242/jeb.105676

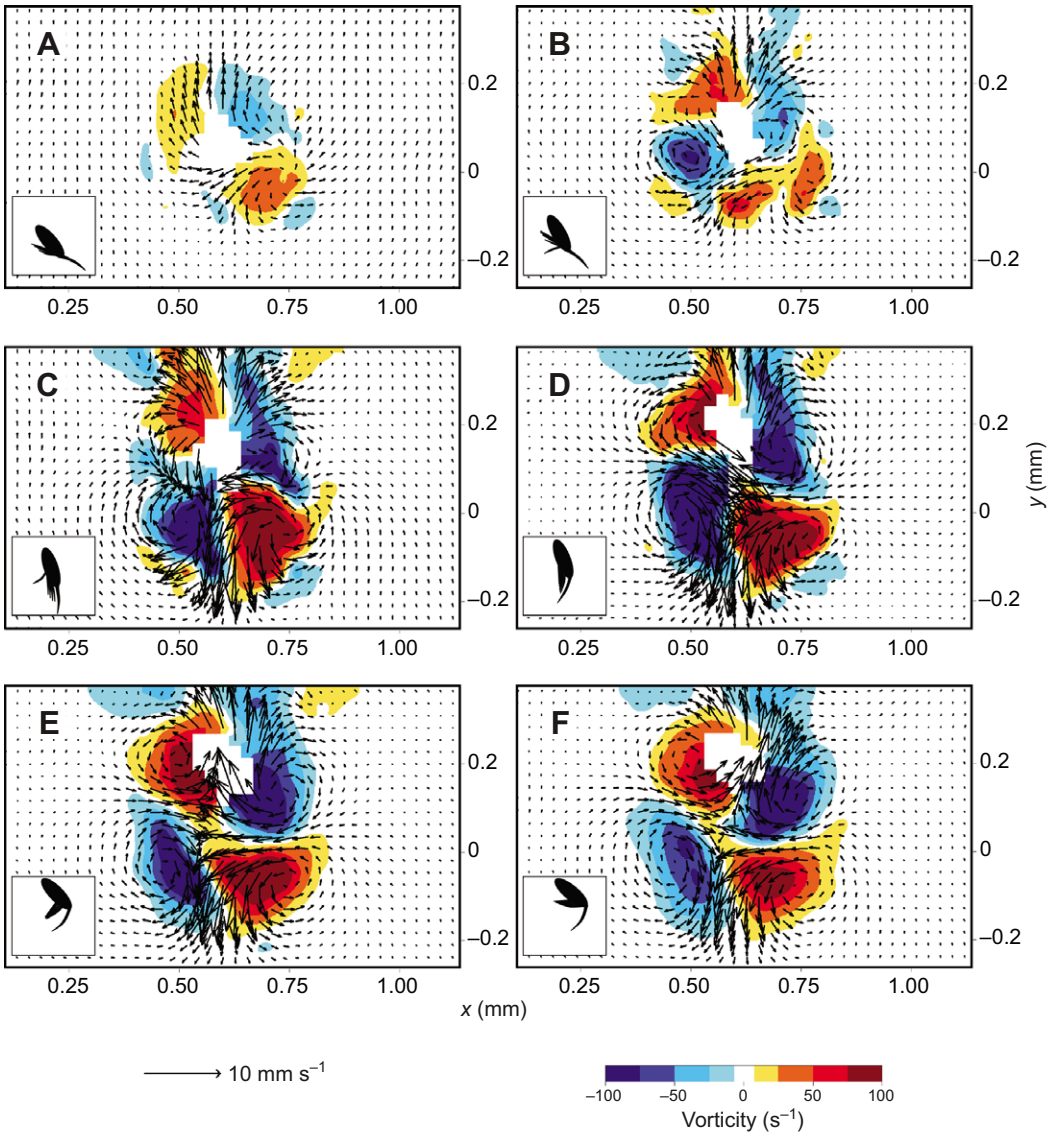

Fig. 3. Time series of the flow fields around a jumping copepodid. L=0.33 mm, T=5 ms, U=61.1 mm s^{-1}, β=18.6, Re=19.1. The position of appendages is shown in the insets and correspond to the stages in Fig. 1. The arrows represent velocity vectors and the colours vorticity, with warm colours for counter-clockwise rotation and cool colours for clockwise rotation. (A–D) Power stroke and (E,F) recovery stroke. Two vortex rings are formed during the jump. Also see supplementary material Movie 2.

Temporal evolution of the fluid disturbance

To characterize the extent of the disturbance created by the copepod, we measured the area of the region around the organism where the velocity exceeded a threshold U_t. We call this area the area of influence S and the characteristic size of the disturbance $R=\sqrt{S}$. In order to quantify how the fluid disturbance grew and decayed in time, we measured S as a function of time t (Fig. 6A). We chose U_t=1 mm s^{-1} so that we were able to measure large enough values of S that they were above the noise level. We then measured the time it takes for S at the end of the power stroke to decay to one-fifth of its value and called it the decay time scale T_{decay} (Fig. 6A). Any disturbance imparted to the fluid is diffused by the effect of viscosity, and the time scale over which this happens is the viscous time scale $T_{visc}=L^2/4\nu$, where L is the characteristic length, the body length in the present case. We compared the measured T_{decay} with T_{visc} and found a one to one correspondence between the two (Fig. 6B).

For nauplii, the disturbance was short lived (10–20 ms), whereas it lasted much longer for the copepodids (20–120 ms). In spite of the significant difference in size, the power stroke duration for nauplii and copepodids was comparable (Table 1). But the viscous decay of the flow was much slower in copepodids owing to their larger size. As a result, the copepodid vortex rings last much longer, even after the recovery stroke, in contrast to those formed by nauplii.

Spatial decay of the fluid disturbance

The spatial extent of the flow disturbance can be quantified by analysing how the size of disturbance R changes with the threshold velocity U_t. Power laws have often been used to describe the attenuation of flow fields generated by swimming organisms (Catton et al., 2007; Jiang and Kiørboe, 2011a; Murphy et al., 2012; Jiang and Kiørboe, 2011b; Visser, 2001; Guasto et al., 2012). To compare our observations with the existing models, we looked for a power law scaling of flow velocity with distance. If $R \sim U_t^{-b}$, then by rearranging the terms, we can find the change in the flow velocity magnitude v_f with distance r from the organism as $v_f \sim r^{-1/b}$.

We measured the size of the fluid disturbance R_0 at the end of the power stroke for different values of U_t ranging between 0.5 mm s^{-1} and 30 mm s^{-1}. Fig. 7A shows the plot of R_0 versus U_t for 50 jumps. At very high values of U_t, the plots plateaued, as the measured area of influence was just the area covered by the organism and the fluid velocity did not exceed U_t anywhere. At the lower end, the measurements were influenced by the background noise. For intermediate values of U_t, the curves can be approximated by a

The Journal of Experimental Biology (2014) doi:10.1242/jeb.105676

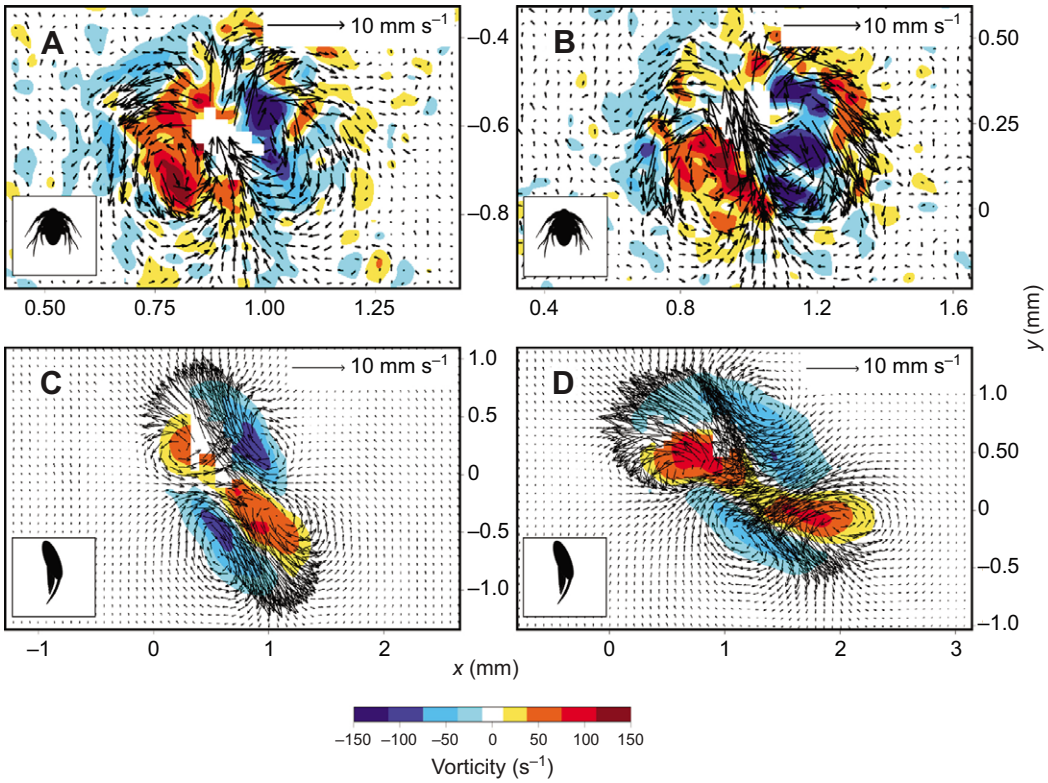

Fig. 4. Snapshots of the flow fields around jumping nauplii and copepodids of different sizes at the end of their power stroke. (A) Small and (B) large nauplii and (C) small and (D) large copepodids. (A) L=0.17 mm, T=7 ms, U=31.1 mm s^{-1}; (B) L=0.26 mm, T=6.5 ms, U=40.5 mm s^{-1}; (C) L=0.55 mm, T=11 ms, U=84.9 mm s^{-1} and (D) L=0.77 mm, T=18.5 ms, U=71.0 mm s^{-1}. The flow structures caused by different sized nauplii are qualitatively similar, with a single toroidal vortex ring, and different from that caused by copepodids, which form two vortex rings.

power law, although it should be kept in mind that the curves are not exactly straight lines on the log–log plot. We selected the range of U_t between 1 mm s^{-1} and 5 mm s^{-1} for calculation of the scaling exponent b, (Fig. 7A, shaded). Fig. 7B shows a scatter plot of b versus β for both nauplii and copepodids. b decreased with β, with a sharp contrast between nauplii and copepodids (Table 2), signifying a faster decay for copepodids than for nauplii.

Energy dissipation

We measured the rate of viscous energy dissipation P around the jumping nauplii and copepodids (Fig. 8A). P grew as the organism accelerated, peaked around the end of the power stroke, and then decayed back to the background level. By integrating the dissipation rate over time, we estimated the total energy dissipated in the fluid. Fig. 8B shows a plot of the energy dissipation per jump W_{diss} (Eqn 13, see Materials and methods) versus β for both nauplii and copepodids. W_{diss} for a nauplius was of the order of 10^{-11} J (Fig. 8B, inset), whereas W_{diss} for a copepodid depended strongly on β and was of the order of 10^{-10} J.

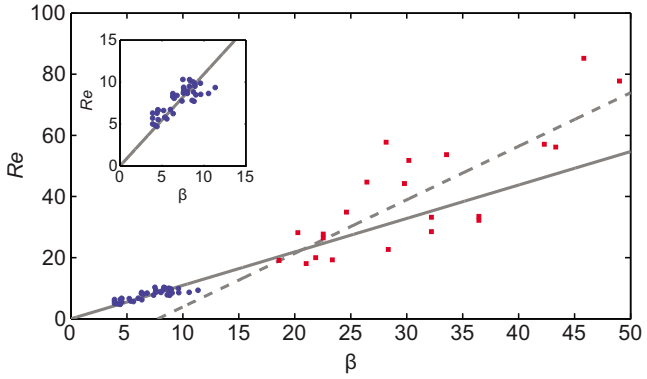

Fig. 5. *Re* versus β for nauplii jumps (blue circles) and copepodid jumps (red squares). The solid line is a straight line fit to the nauplii data (slope=1.09±0.06, R^2=0.38, forced through the origin). The inset shows a zoom on the nauplii data. The dashed line is the best fit for the copepodid data (slope=1.75±0.59, R^2=0.66, *Re*-intercept=–13.6±18.6). Nauplii and copepodid data form two groups, which clearly separate from each other on both the axes (Table 1).

DISCUSSION

Flow field structure

Flow velocimetry has previously been employed to measure the flows around adult copepods (Jiang and Kiørboe, 2011a; Murphy et al., 2012; van Duren et al., 2003). Here, for the first time, we have extended the use of these techniques to measure the flows caused by nauplii. The measured velocity fields showed that the flows induced in the vicinity of a jumping nauplius and a copepodid are qualitatively different from each other (Fig. 4). The induced flow around a nauplius consists of a single vortex ring, in contrast to the two counter-rotating vortex rings observed around copepodids, and this distinction is independent of the finer details of the flow or how well formed the respective flow structures are. The flow structure

Table 1. Quantities measured from kinematic analysis of videos

	Nauplius		Copepodid	
	Mean	Range	Mean	Range
N	41	n.a.	22	n.a.
L (mm)	0.22	0.17–0.26	0.48	0.33–0.77
T (ms)	6.8	5.5–8.5	7.8	3.5–18.5
U (mm s^{-1})	37.4	28.5–46.1	83.9	57.1–129.0
β	7.0	3.9–10.3	30.4	18.6–49.0
Re	7.9	4.7–10.3	39.6	18.0–85.2

L, T and U are the body length, power stroke duration and maximum swimming velocity, respectively. β is the frequency parameter and *Re* is the Reynolds number.

The Journal of Experimental Biology (2014) doi:10.1242/jeb.105676

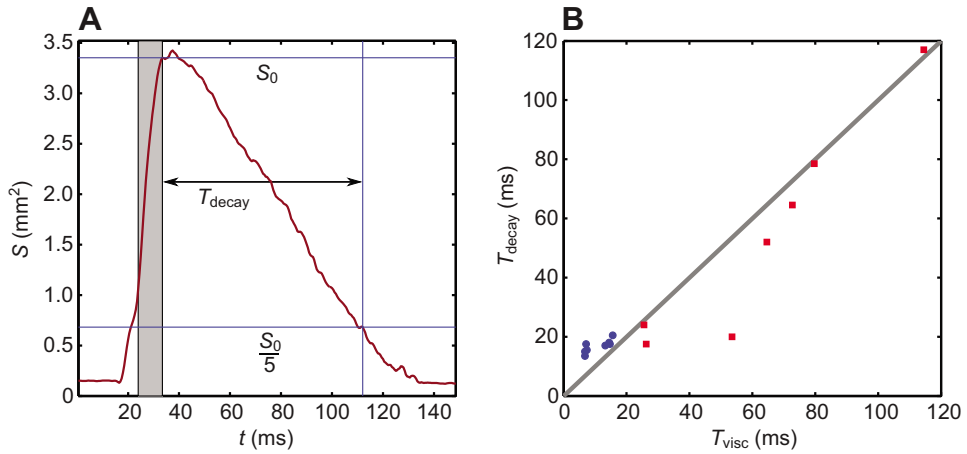

Fig. 6. Time scales associated with a jump. (A) Evolution of the area of influence S with time t for a copepodid (L=0.58 mm, T=9.5 ms, U=97.4 mm s^{-1}). The shaded area represents the power stroke starting with the movement of the swimming legs. The decay time T_{decay} is measured from the end of the power stroke to the instant when S has decreased to a fifth of its value S_0 at the end of the power stroke. (B) Decay time T_{decay} versus the viscous time scale T_{visc}. Blue circles are for nauplii data (N=8) and red squares are for copepodids (N=7). The straight line represents a one to one relationship.

around jumping copepodids is similar to the flow structure observed around adults in this and in other species (Jiang and Kiørboe, 2011a; Murphy et al., 2012; Yen and Strickler, 1996).

The difference between the nauplii and copepodids could either be due to the differences in morphology and propulsion mechanism, or due also to the hydrodynamical difference in the relative importance of viscosity and inertia. The nauplii flow pattern results from a combination of forces acting on the fluid in different directions – the appendages pushing the fluid backwards on each side of the body, and the drag acting on the body pushing the fluid forward. This force configuration is typical for breaststroke swimmers. In copepodids, by contrast, all propulsive forces are applied in one region by the swimming legs pushing the fluid backwards, while the drag on the body pushes the fluid forward. Owing to higher inertia in copepodids than in nauplii, viscosity does not diffuse the momentum away, and the fluid rolls up into vortices both in the front of the organism and in the wake, leading to the two vortex rings observed (Jiang and Kiørboe, 2011a).

The linear relationship between β and Re for nauplii (Fig. 5) suggests that the velocity and frequency scale for nauplii jumps are linearly related through the size of the organism. Even though the values of Re for nauplii are larger than unity, the proportionality expected from low Reynolds number swimming still holds to a large extent. A slope of ~1 indicates that a nauplius moving at peak velocity covers approximately one body length per power stroke, irrespective of the size and developmental stage. In the case of copepodids, the slope was 1.75, which shows that the copepodids cover more body lengths in each jump than the nauplii do. The slope of the Re–β plot is equal to UT/L, i.e. the inverse of the Strouhal number. The value for T was not significantly higher in copepodids than in nauplii (Table 1). Thus, the higher slope for copepodids, in spite of higher L, is mainly due to their higher swimming velocity U, showing that they are more effective swimmers than nauplii.

Decay of the flow disturbance

The fluid disturbance caused by the jump of a nauplius or a copepodid determines the predation risk associated with their

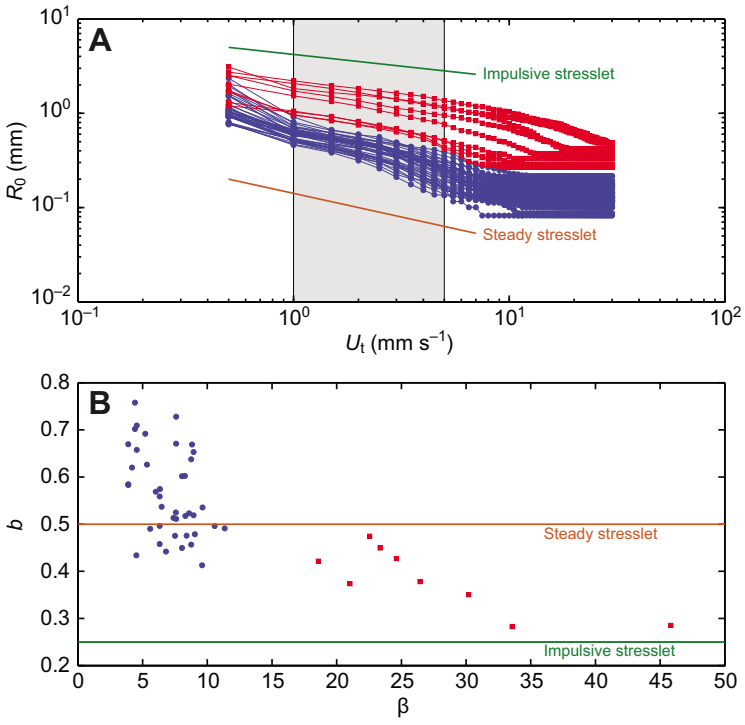

Fig. 7. Spatial decay of the fluid disturbance. (A) Size of the fluid disturbance R_0 measured at the end of the power stroke, versus U_t. Blue lines with circles are for nauplii data (N=41) and red lines with squares are for copepodids (N=9). The part of the plot used for power law fits is shaded in grey. The green and orange lines have scaling exponents equal to those of an impulsive stresslet (b=1/4) and a steady stresslet (b=1/2), respectively. (B) Scaling exponent b for the curves in A plotted against the frequency parameter β. Blue circles are for nauplii and red squares for copepodids.

The Journal of Experimental Biology (2014) doi:10.1242/jeb.105676

Table 2. Quantities measured from the flow fields

	Nauplius			Copepodid		
	N	Mean	Range	*N*	Mean	Range
T_{decay} (ms)	8	16.8	13.5–20.5	7	53.4	17.5–117
T_{visc} (ms)	8	10.8	6.8–15.6	7	62.4	25.6–114.5
Spatial decay exponent, *b*	41	0.56	0.41–0.75	9	0.38	0.28–0.47
W_{diss} (10^{-11} J)	12	3.77	2.56–5.35	7	20.6	1.2–66.9
W_{drag} (10^{-11} J)	12	0.95	0.53–1.42	7	19.3	2.2–70.2

T_{decay} and T_{visc} are the measured decay time scale of the flow disturbance and the viscous time scale, respectively. *b* is the exponent for spatial decay of the velocity field. W_{diss} is the energy dissipated in the fluid per jump, and W_{drag} is the useful work done against the drag force.

locomotion. Most rheotactic predators respond to disturbances exceeding only a certain threshold velocity (Kiørboe and Visser, 1999). The spatial and temporal decay rate is an important feature of the disturbance, which determines how far and for how long the organism stays vulnerable. We found that the temporal decay of the disturbance was controlled by the viscous time scale dictated by the size of the organism. At the small spatial scales involved, viscous diffusion acts as the main process responsible for the decay of fluid motion. The viscous time scale varies with the square of the length scale. As the nauplii have a body size much smaller than the copepodids, the disturbance created by them is dissipated much faster than that by the copepodids (Fig. 6; Table 2).

The spatial decay of the disturbance is characterized by the exponent of the power law used to describe the disturbance. The rate of decay and hence the exponent is different in the case of nauplii and copepodids (Fig. 7). The smaller magnitude of *b* for copepodids than for nauplii implies a faster decay of velocity with distance from the organism, as $v_f \sim r^{-1/b}$.

The exponent for the decay allows us to compare it with the idealized singularity models (Table 3), which are often used to model the flows generated by organisms swimming at low Reynolds numbers (Jiang and Kiørboe, 2011a; Jiang and Kiørboe, 2011b; Visser, 2001; Guasto et al., 2012; Murphy et al., 2012; Catton et al., 2007; Drescher et al., 2011). For example, a continuously moving free-swimming organism at low Reynolds number is often represented by a steady stresslet, which consists of two equal magnitude forces acting on the fluid in opposite directions, a small distance away from each other (Guasto et al., 2012; Visser, 2001). Also, unsteady jumps of adult copepods have been modelled using an impulsive stresslet model, in which the two forces act impulsively on the fluid (Jiang and Kiørboe, 2011a; Murphy et al., 2012). The range of *b* measured for the nauplii is comparable with the steady stresslet model, given the experimental variability and noise in the data. This suggests that the unsteadiness of the motion may be less important in case of nauplii and that the flow behaves in a more quasi-steady fashion, probably because of their small size and correspondingly small values of the frequency parameter β. In contrast, the values of *b* for copepodids approach the value expected for an impulsive stresslet, especially at higher values of β, emphasizing the unsteady nature of the jump.

The range of data available for curve fitting (Fig. 7A) was too small to draw strong conclusions about the exact model capturing the decay, but the relative difference between nauplii and copepodids is clear (Fig. 7B). We note that the comparison of nauplii swimming with a steady stresslet is limited to the far field spatial decay of the flow velocity, because the observed toroidal flow structure is incompatible with a steady stresslet. It is possible that the nauplius flow field is a combination of fundamental singularities

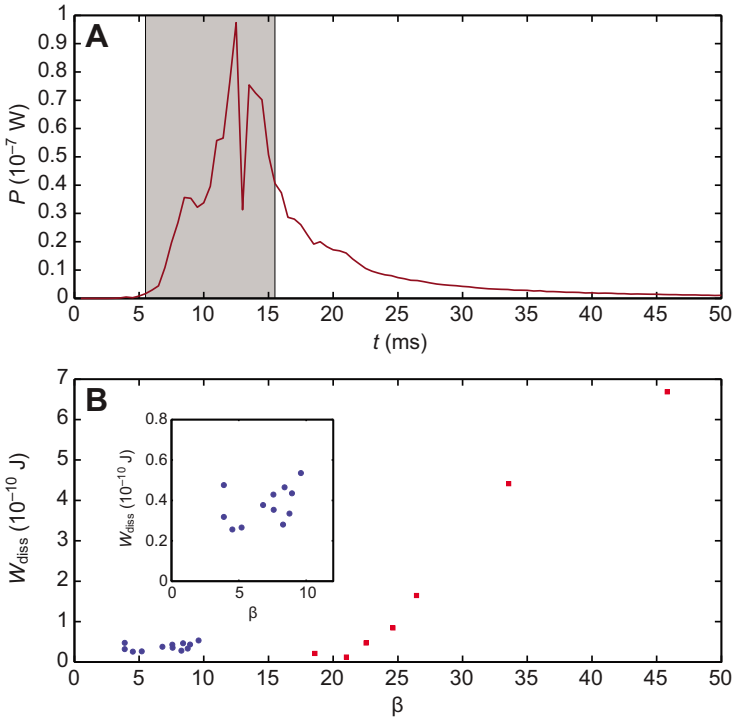

Fig. 8. Viscous energy dissipation during a copepod jump. (A) Energy dissipation rate *P* around a copepodid as a function of time *t* (*L*=0.69 mm, *T*=10 ms, *U*=129.0 mm s^{-1}). The shaded area represents the power stroke starting with the movement of the swimming legs. (B) Dissipation per jump W_{diss} versus β for nauplii (blue circles, *N*=12) and copepodids (red squares, *N*=7). The inset shows a zoom on the nauplii data.

Table 3. The spatial decay exponent, *b*, measured for nauplii and copepodids, compared with idealized point force models

	Nauplii	Copepodids	Steady stresslet	Impulsive stresslet
b	0.56 (0.41–0.75)	0.38 (0.28–0.47)	1/2	1/4

and that the near field flow structure is dominated by other singularities, which decay faster with distance than a stresslet, resulting in the far field decay being described solely by a stresslet. Other factors, such as the complex shape of the organism and intermediate Reynolds numbers, might also make a pure stresslet model incompatible with the observations, motivating the development of new and more realistic models.

Energy budget

To compare the energy expenditure on swimming to the metabolic budget of the copepod, we used the metabolic rate scaling for calanoid copepods given in terms of the carbon mass as $R_m=3.46M^{-0.22}$, where R_m is the mass specific metabolic rate in $mlO_2\ mgC^{-1}\ h^{-1}$ and M is the mass of the organism in mgC (Kiørboe and Hirst, 2014). The carbon mass of nauplii varies between 30 and 250 ngC so we use a value of 100 ngC to get an order of magnitude estimate (Berggreen et al., 1988). Using an oxycalorific value of 13.8 J mgC^{-1}, we got a metabolic rate of 1.44×10^{-5} W for nauplii. With this metabolic rate, the energy budget of a nauplius over the duration of a typical jump (10 ms) is of the order of 10^{-7} J. Thus, the energy spent by a nauplius on swimming (~10^{-11} J) is approximately four orders of magnitude smaller than the metabolic budget. The same conclusion is applicable to copepodids, for which the swimming and metabolic budgets are of the order of 10^{-10} J and 10^{-6} J, respectively.

Many previous studies have made the same conclusion, for a range of swimming organisms, such as copepods (van Duren et al., 2003; Vlymen, 1970) and protists (Crawford, 1992). However, the above estimate does not take into account the losses involved at the different stages of energy conversion, which might have a significant effect on the net cost of propulsion. This could explain the observations made previously on copepods and larger crustaceans, which showed a significant increase in the metabolic rate of the organism during locomotion activity (Halcrow and Boyd, 1967; Torres and Childress, 1983; Svetlichny and Hubareva, 2005; Buskey, 1998). High propulsion costs would drive evolution towards optimizing swimming, something that has been proposed for other organisms (Spagnolie and Lauga, 2011; Tam and Hosoi, 2011).

Propulsion efficiency

Another interesting aspect of the energy expenditure of nauplii and copepodids is the efficiency of swimming. The conventional measure of efficiency is the so-called Froude efficiency $\eta_F=W_{drag}/W_{diss}$, which compares the total swimming work done by an organism W_{diss}, to the useful part of the work W_{drag}, which is done by the thrust forces against the drag on the organism. To estimate W_{drag}, we approximated the copepod with a sphere moving through water with the same kinematics as the real organism. An alternative approximation of a copepod body as a prolate spheroid results only in small quantitative differences, and for simplicity we chose the sphere approximation. We used the width of the copepod at the thickest part of the prosome as the diameter of the sphere, D, calculated from the body length L using the aspect ratios of 0.5 and 0.38 for nauplii and copepodids, respectively (Kiørboe et al., 2010; Andersen Borg et al., 2012). We thus modelled the drag (F_d) on the copepod using the quasi-steady expression,

$$F_d=\frac{1}{2}\pi\rho C_d\left(\frac{D}{2}\right)^2 V^2, \quad (8)$$

where V is the instantaneous swimming velocity. Following Lautrup (Lautrup, 2005), the drag coefficient (C_d) depends on the instantaneous Reynolds number for the sphere, $Re_s=DV/\nu$, as:

$$C_d=\frac{24}{Re_s}+\frac{5}{\sqrt{Re_s}}+0.4. \quad (9)$$

W_{drag} is calculated by integrating the drag power F_dV over the whole duration of motion, divided by the number of jumps. Fig. 9 compares W_{drag} to the energy dissipation per jump W_{diss}. The straight line in Fig. 9 represents a one to one proportionality and corresponds to 100% Froude efficiency described above. The data for copepodids were close to the 100% line (Fig. 9A), whereas those for nauplii were all much below the line (Fig. 9B). The value of the Froude efficiency for copepods was 1.19±0.40. Our measurements validate the predictions made from computational fluid dynamics calculations that the copepod jumps have a high Froude efficiency (Jiang and Kiørboe, 2011b). In comparison, the Froude efficiency for nauplii was 0.26±0.08. Thus, nauplii are energetically much less efficient in propulsion than the copepodids. Copepods swim at Reynolds numbers several orders of magnitude higher than that of most micro-organisms, and consequently, the swimming efficiency of both nauplii and copepodids was much higher than what has been predicted and measured for micro-organisms (Guasto et al., 2012). The dissipation is likely to have been underestimated due to the limited resolution of the PIV data, so the actual Froude efficiency is presumably less than that calculated here.

This way of calculating the efficiency requires one to be able to unambiguously separate the swimming forces into thrust and drag, which is often not possible for organisms swimming at intermediate or high Reynolds numbers. Even at low Reynolds numbers, where drag and thrust are unambiguously distinguishable, the above

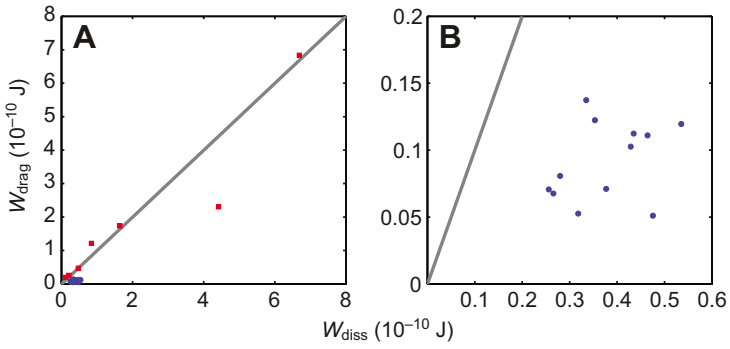

Fig. 9. Propulsion efficiency. (A) The useful work W_{drag} done in overcoming drag versus the dissipation per jump W_{diss} for nauplii (blue circles, N=12) and copepodids (red squares, N=7). The straight line represents W_{drag} = W_{diss}, corresponding to 100% Froude efficiency. (B) A zoom on the nauplii jump data.

mentioned efficiency remains an ill-defined concept and can take arbitrarily large values (Childress, 2012; Leshansky et al., 2007). Thus, one needs to be careful when interpreting the Froude efficiency. Nevertheless, the above calculations demonstrate a significant difference between nauplii and copepodids.

It has been suggested that the nauplii have a body shape that is optimized for swimming at Reynolds number around unity (Andersen Borg et al., 2012). But this optimality in body shape changes with increase in size and a corresponding increase in the Reynolds numbers, and a more elongated body is preferred. It appears that the copepodid body plan and swimming stroke are also well suited for its physical environment and allow it to achieve a higher swimming efficiency. Thus, the hydrodynamic changes associated with changing size might explain the stark physical differences between nauplii and copepodids.

The breaststroke swimming gait used by copepod nauplii studied here is common among many aquatic organisms of diverse taxa and sizes, but its hydrodynamics are not well understood, and physically realistic models are needed. It is important that any such models capture the flow close to the organism, because the dominant flow structures and energy dissipation are observed here. We hope that the measurements presented here can be used for developing accurate intermediate Reynolds number models for flows around nauplii and copepodids.

MATERIALS AND METHODS

Experimental set-up

Copepods *Acartia tonsa* were cultured at 18°C. Before experiments, we transferred the copepods to the test aquarium that contained filtered sea water. We added only a few individuals to the aquarium in order to avoid any interaction between them. All experiments were conducted in a glass cuvette (1×1×4 cm) placed on a horizontal translation stage, at room temperature between 18°C and 20°C.

A vertical plane within the cuvette, orthogonal to the camera view, was illuminated by an infrared pulsed laser (808 nm wavelength) (Oxford Lasers Ltd, Oxon, UK) with a 150 µm thick light sheet. We used a Phantom v210 high-speed digital video camera (Vision Research, Inc., Wayne, New Jersey, USA), at a frame rate of 2000 frames s^{-1} and a resolution of 1280×800 pixels. The laser and the camera were synchronised. The camera was fitted with an inverted 20 mm focal length lens (Nikon Corporation, Tokyo, Japan) and a magnifying bellows tube to achieve a field of view ranging between 3.0 and 20.5 mm^2.

For PTV and PIV seeding, we prepared a suspension of TiO_2 particles by suspending a small amount of TiO_2 powder in ethanol and diluting it with filtered sea water, followed by treatment with ultrasound for 1 h, yielding particles smaller than 2 µm (Riisgård et al., 2011). We then added a small amount of the suspension to the aquarium to achieve an appropriate seeding density. The organisms were not affected by the presence of infrared light or seeding particles.

Kinematic analysis

Using the MATLAB-based image analysis software DLTdv5 (Hedrick, 2008), we digitized two ends of the prosome in order to measure the body size (L) and to establish the length axis. The mid-point of these two points was used for calculating the swimming velocity using a finite difference scheme. We smoothed the velocity data using a Savitzky–Golay smoothing filter (Savitzky and Golay, 1964). For each jump, we measured the duration of the power stroke (T). For nauplii, T was taken to be the time from the beginning of antennae movement to the end of the downward motion of the antennules. For copepodids and adults, acceleration started with movement of the antennae, but the main thrust was produced by the swimming legs. Thus, we measured T as the time taken for the backward motion of the swimming legs. A total of 63 jumps were analysed (Table 1), out of which 50 were used for further calculations based on flow fields. The rest were not used for flow field calculations due to misalignment between the plane of the laser sheet and the centreline of the copepod body.

Velocimetry

We used PTV for measuring the flows created by nauplii and PIV for the flows around copepodids (Raffel, 2007). For both, we used the software Davis (LaVision GmbH, Göttingen, Germany) for capturing and analysing the recordings. In PIV analyses, we used a multi-pass algorithm with decreasing size of the interrogation windows, with a final window size of 32×32 pixels with a 50% overlap. We used an algorithmic mask, consisting of a sliding averaging of the intensity values followed by thresholding to remove those pixels from the analysis that corresponded to the organism. The process of masking made it impossible for us to measure the flows right next to the organism, especially around the swimming appendages. We adjusted the masking parameters for each recording to minimize the loss of useful data. After every pass of the processing and during post-processing, we removed outlying velocity vectors using a median filter and de-noising.

We used a combined PIV+PTV method for the flow field measurements around jumping nauplii. A coarse grid (64×64 pixels) PIV calculation was used as the initial guess for the PTV. The velocity field obtained from PTV was passed through a median filter followed by de-noising. We then converted the resulting vector field to a grid with window size 16×16 pixels to achieve the same vector density as that in the PIV calculations described above.

Energy dissipation

For any swimming organism, all the energy supplied to the fluid eventually dissipates as heat, which is due to viscosity. For an incompressible Newtonian fluid, the rate of strain tensor, ε_{ij}, and the rate of viscous energy dissipation per unit volume, ϕ, called the viscous dissipation function, are given as (Batchelor, 1967):

$$\varepsilon_{ij} = \frac{1}{2}\left(\frac{\partial v_i}{\partial x_j} + \frac{\partial v_j}{\partial x_i}\right), \tag{10}$$

$$\phi = 2\mu\varepsilon_{ij}\varepsilon_{ij}. \tag{11}$$

The total energy dissipation rate P in a volume V is found by integrating ϕ over the volume,

$$P = \int_V \phi \mathrm{d}V. \tag{12}$$

In a series of n jumps, the energy supplied to the fluid by the copepod per jump (W_{diss}) is found by integrating P over the whole duration of motion (T_{end}) and dividing by the number of jumps,

$$W_{diss} = \frac{1}{n}\int_0^{T_{end}} P \mathrm{d}t. \tag{13}$$

We assume that the flow field is rotationally symmetric about the direction of jump and use a cylindrical polar coordinate system, such that the z-axis is aligned with the direction of swimming at peak velocity of the organism. The assumption of rotational symmetry is invalid in the close vicinity of the organism, as the body plan and swimming strokes are clearly not rotationally symmetric, but it allows us to integrate over the entire volume around the organism to include the observed vortex rings. For a rotationally symmetric flow, in the absence of swirl about the symmetry axis, the viscous dissipation function ϕ can be written in cylindrical polar coordinates as (Batchelor, 1967):

$$\phi = \mu\left[2\left\{\left(\frac{\partial v_r}{\partial r}\right)^2 + \left(\frac{v_r}{r}\right)^2 + \left(\frac{\partial v_z}{\partial z}\right)^2\right\} + \left(\frac{\partial v_r}{\partial z} + \frac{\partial v_z}{\partial r}\right)^2\right]. \tag{14}$$

We expect Eqn 14 to give a better estimate of the viscous energy dissipation around a jumping copepod, than the approximate expressions used in previous studies (van Duren et al., 2003; Catton et al., 2007). The volume integration in Eqn 12 was performed by integrating the planar measurements over the azimuthal angle, assuming rotational symmetry. To remove the background noise level of dissipation from the measurement, we

removed those regions from the integration where the flow velocity was below a threshold of 0.5 mm s^{-1}.

Acknowledgements
We would like to thank Rodrigo Gonçalves, Jack Melbye, Lone Gram, Knud Erik Meyer, Pavlos Vlachos and Danny Grünbaum for their help and advice at different stages of this research.

Competing interests
The authors declare no competing financial interests.

Author contributions
N.W., A.A. and T.K. conceived the research and designed experiments; N.W. collected and analysed data; N.W., A.A. and T.K. interpreted results. N.W. and A.A. drafted the article and all authors revised it.

Funding
The Centre for Ocean Life is a Villum Kann Rasmussen Centre of Excellence supported by the Villum Foundation.

Supplementary material
Supplementary material available online at
http://jeb.biologists.org/lookup/suppl/doi:10.1242/jeb.105676/-/DC1

References

Andersen Borg, C. M., Bruno, E. and Kiørboe, T. (2012). The kinematics of swimming and relocation jumps in copepod nauplii. *PLoS ONE* **7**, e47486.
Batchelor, G. K. (1967). *An Introduction to Fluid Dynamics*. Cambridge, UK: Cambridge University Press.
Berggreen, U., Hansen, B. and Kiørboe, T. (1988). Food size spectra, ingestion and growth of the copepod *Acartia tonsa* during development: Implications for determination of copepod production. *Mar. Biol.* **99**, 341-352.
Buskey, E. J. (1998). Energetic costs of swarming behavior for the copepod *Dioithona oculata*. *Mar. Biol.* **130**, 425-431.
Catton, K. B., Webster, D. R., Brown, J. and Yen, J. (2007). Quantitative analysis of tethered and free-swimming copepodid flow fields. *J. Exp. Biol.* **210**, 299-310.
Childress, S. (2012). A thermodynamic efficiency for Stokesian swimming. *J. Fluid Mech.* **705**, 77-97.
Childress, S. and Dudley, R. (2004). Transition from ciliary to flapping mode in a swimming mollusc: flapping flight as a bifurcation in Re_{ω}. *J. Fluid Mech.* **498**, 257-288.
Crawford, D. W. (1992). Metabolic cost of motility in planktonic protists: Theoretical considerations on size scaling and swimming speed. *Microb. Ecol.* **24**, 1-10.
Drescher, K., Dunkel, J., Cisneros, L. H., Ganguly, S. and Goldstein, R. E. (2011). Fluid dynamics and noise in bacterial cell-cell and cell-surface scattering. *Proc. Natl. Acad. Sci. USA* **108**, 10940-10945.
Guasto, J. S., Rusconi, R. and Stocker, R. (2012). Fluid mechanics of planktonic microorganisms. *Annu. Rev. Fluid Mech.* **44**, 373-400.
Halcrow, K. and Boyd, C. M. (1967). The oxygen consumption and swimming activity of the amphipod *Gammarus oceanicus* at different temperatures. *Comp. Biochem. Physiol.* **23**, 233-242.
Hedrick, T. L. (2008). Software techniques for two- and three-dimensional kinematic measurements of biological and biomimetic systems. *Bioinspir. Biomim.* **3**, 034001.
Jiang, H. and Kiørboe, T. (2011a). The fluid dynamics of swimming by jumping in copepods. *J. R. Soc. Interface* **8**, 1090-1103.
Jiang, H. and Kiørboe, T. (2011b). Propulsion efficiency and imposed flow fields of a copepod jump. *J. Exp. Biol.* **214**, 476-486.
Kiørboe, T. and Hirst, A. G. (2014). Shifts in mass scaling of respiration, feeding, and growth rates across life-form transitions in marine pelagic organisms. *Am. Nat.* **183**, E118-E130.
Kiørboe, T. and Jiang, H. (2013). To eat and not be eaten: optimal foraging behaviour in suspension feeding copepods. *J. R. Soc. Interface* 10, 20120693.
Kiørboe, T. and Visser, A. (1999). Predator and prey perception in copepods due to hydromechanical signals. *Mar. Ecol. Prog. Ser.* **179**, 81-95.
Kiørboe, T., Andersen, A., Langlois, V. J. and Jakobsen, H. H. (2010). Unsteady motion: escape jumps in planktonic copepods, their kinematics and energetics. *J. R. Soc. Interface* **7**, 1591-1602.
Larink, O. and Westheide, W. (2006). *Coastal Plankton. Photo Guide for European Seas*. München, Germany: Pfeil.
Lauga, E. and Powers, T. R. (2009). The hydrodynamics of swimming microorganisms. *Rep. Prog. Phys.* **72**, 096601.
Lautrup, B. (2005). *Physics of Continuous Matter*. Bristol, UK: Institute of Physics Publishing.
Leshansky, A. M., Kenneth, O., Gat, O. and Avron, J. E. (2007). A frictionless microswimmer. *New J. Phys.* **9**, 145.
McHenry, M. J., Azizi, E. and Strother, J. A. (2003). The hydrodynamics of locomotion at intermediate Reynolds numbers: undulatory swimming in ascidian larvae (*Botrylloides sp.*). *J. Exp. Biol.* **206**, 327-343.
Murphy, D., Webster, D. and Yen, J. (2012). A high-speed tomographic PIV system for measuring zooplanktonic flow. *Limnol. Oceanogr. Methods* **10**, 1096-1112.
Nybakken, J. W. and Bertness, M. D. (2005). *Marine Biology: an Ecological Approach*, 6th edn. San Francisco, CA: Benjamin Cummings.
Pozrikidis, C. (2011). *Introduction to Theoretical and Computational Fluid Dynamics*, 2nd edn. Oxford, UK: Oxford University Press.
Raffel, M. (2007). *Particle Image Velocimetry: A Practical Guide*, 2nd edn. Heidelberg, Germany: Springer.
Riisgård, H. U., Jørgensen, B. H., Lundgreen, K., Storti, F., Walther, J. H., Meyer, K. E. and Larsen, P. S. (2011). The exhalant jet of mussels *Mytilus edulis*. *Mar. Ecol. Prog. Ser.* **437**, 147-164.
Savitzky, A. and Golay, M. J. E. (1964). Smoothing and differentiation of data by simplified least squares procedures. *Anal. Chem.* **36**, 1627-1639.
Sensenig, A. T., Kiger, K. T. and Shultz, J. W. (2009). The rowing-to-flapping transition: ontogenetic changes in gill-plate kinematics in the nymphal mayfly centroptilum triangulifer (Ephemeroptera, Baetidae). *Biol. J. Linn. Soc. Lond.* **98**, 540-555.
Spagnolie, S. E. and Lauga, E. (2011). Comparative hydrodynamics of bacterial polymorphism. *Phys. Rev. Lett.* **106**, 058103.
Svetlichny, L. S. and Hubareva, E. S. (2005). The energetics of *Calanus euxinus*: locomotion, filtration of food and specific dynamic action. *J. Plankton Res.* **27**, 671-682.
Tam, D. and Hosoi, A. E. (2011). Optimal feeding and swimming gaits of biflagellated organisms. *Proc. Natl. Acad. Sci. USA* **108**, 1001-1006.
Torres, J. and Childress, J. (1983). Relationship of oxygen consumption to swimming speed in *Euphausia pacifica*. *Mar. Biol.* **74**, 79-86.
Turner, J. T. (2004). The importance of small planktonic copepods and their roles in pelagic marine food webs. *Zool. Stud.* **43**, 255-266.
van Duren, L. A. and Videler, J. J. (2003). Escape from viscosity: the kinematics and hydrodynamics of copepod foraging and escape swimming. *J. Exp. Biol.* **206**, 269-279.
van Duren, L. A., Stamhuis, E. J. and Videler, J. J. (2003). Copepod feeding currents: flow patterns, filtration rates and energetics. *J. Exp. Biol.* **206**, 255-267.
Verity, P. and Smetacek, V. (1996). Organism life cycles, predation, and the structure of marine pelagic ecosystems. *Mar. Ecol. Prog. Ser.* **130**, 277-293.
Visser, A. (2001). Hydromechanical signals in the plankton. *Mar. Ecol. Prog. Ser.* **222**, 1-24.
Vlymen, W. J. (1970). Energy expenditure of swimming copepods. *Limnol. Oceanogr.* **15**, 348-356.
Vogel, S. (1994). *Life in Moving Fluids: The Physical Biology of Flow*. Princeton, NJ: Princeton University Press.
Yen, J. and Strickler, J. R. (1996). Advertisement and concealment in the plankton: What makes a copepod hydrodynamically conspicuous? *Invertebr. Biol.* **115**, 191-205.

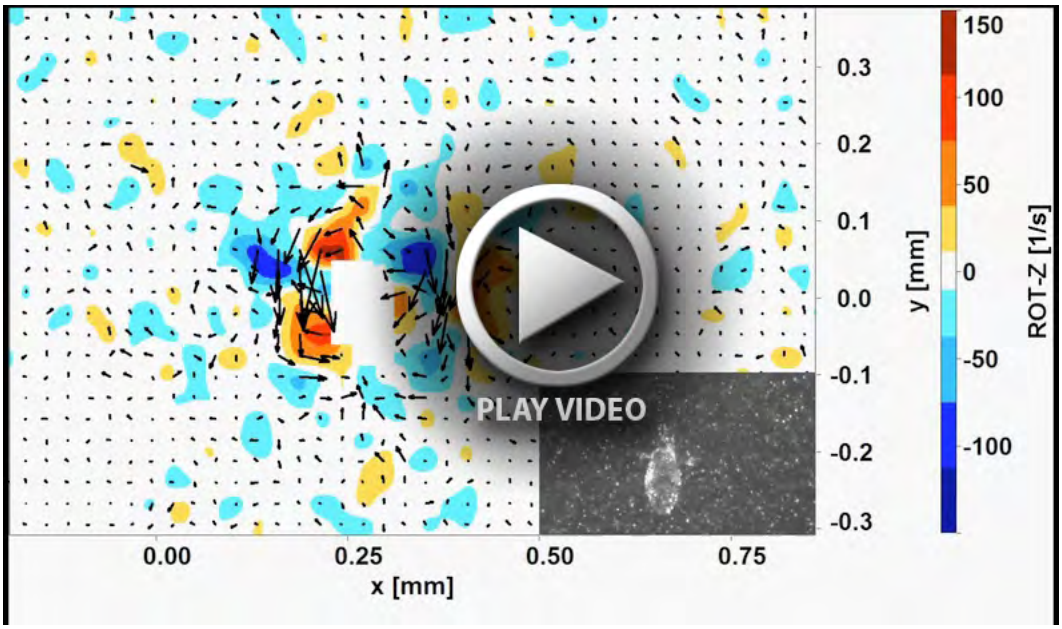

Movie 1: Flow fields around a jumping nauplius, same as in Fig. 2 ($L = 0.24$ mm, $T = 7.5$ ms, $U = 33.7$ mm/s, $\beta = 7.4$, Re $= 7.7$). The panel shows the raw video.

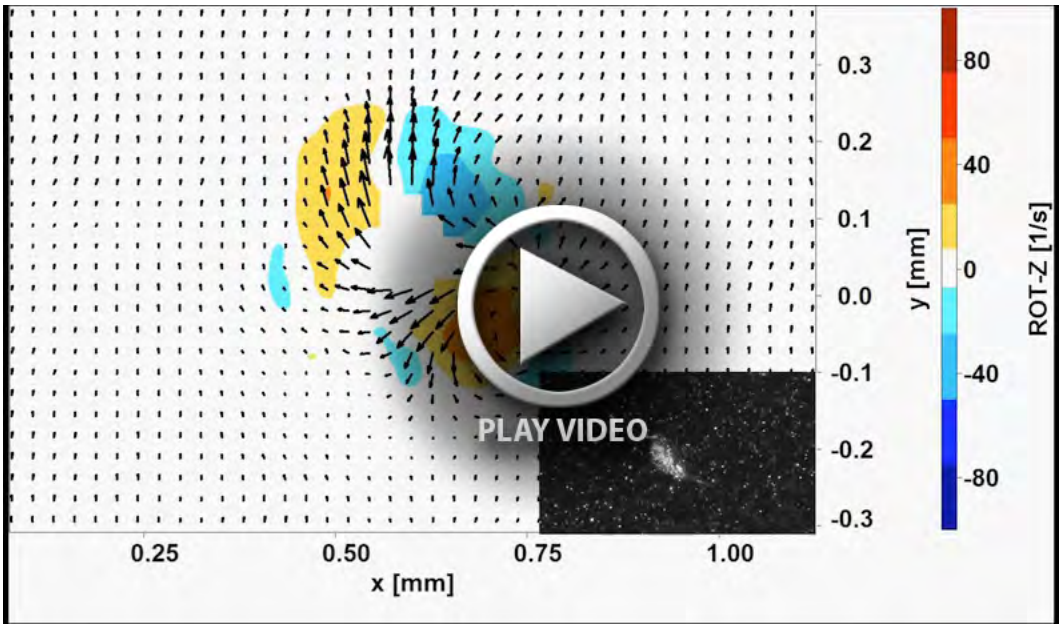

Movie 2: Flow fields around a jumping copepodid, same as in Fig. 3 ($L = 0.33$ mm, $T = 5$ ms, $U = 61.1$ mm/s, $\beta = 18.6$, Re $= 19.1$). The panel shows the raw video.